Gradual inlet expansion and barrier drowning under most sea level rise scenarios

Laura Portos-Amill[1], Jaap H Nienhuis[1], and Huib de Swart[1]

[1]Utrecht University

December 15, 2023

Posted on 30 Nov 2022 — CC-BY 4.0 — https://doi.org/10.1002/essoar.10512944.1 — This is a preprint. Version of Record available at https://doi.org/10.1029/2022JF007010

Check for updates

JGR Earth Surface

RESEARCH ARTICLE
10.1029/2022JF007010

Special Section:
Prediction in coastal geomorphology

Gradual Inlet Expansion and Barrier Drowning Under Most Sea Level Rise Scenarios

Laura Portos-Amill[1,2], Jaap H. Nienhuis[3], and Huib E. de Swart[1]

[1]Department of Physics, Institute for Marine and Atmospheric Research, Utrecht University, Utrecht, The Netherlands, [2]Water Engineering and Management, University of Twente, Enschede, The Netherlands, [3]Department of Physical Geography, Utrecht University, Utrecht, The Netherlands

Key Points:

- Idealized morphological model simulations show that tidal inlets expand until barrier islands disappear under rapid sea level rise
- Modeled barrier drowning lags sea level rise acceleration by 100s of years
- Lag in modeled barrier drowning is explained by a decrease in the sand volume of the barrier

Supporting Information:

Supporting Information may be found in the online version of this article.

Correspondence to:

L. Portos-Amill,
l.portosamill@utwente.nl

Citation:

Portos-Amill, L., Nienhuis, J. H., & de Swart, H. E. (2023). Gradual inlet expansion and barrier drowning under most sea level rise scenarios. *Journal of Geophysical Research: Earth Surface*, *128*, e2022JF007010. https://doi.org/10.1029/2022JF007010

Received 24 NOV 2022
Accepted 22 OCT 2023

© 2023. The Authors.
This is an open access article under the terms of the Creative Commons Attribution License, which permits use, distribution and reproduction in any medium, provided the original work is properly cited.

Abstract The expected increase in rates of sea level rise during the 21st century and beyond may cause barrier islands to drown. Barrier drowning occurs due to a sediment imbalance induced by sea level rise, causing inlets to open and expand. It is still unclear how fast barrier islands can drown. To gain insight into the morphodynamics of barrier systems subject to sea level rise, we here present results obtained with a novel barrier island exploratory model, BarrieR Inlet Environment-Drowning, that considers inlet expansion beyond equilibrium size. We quantify how much of a barrier island chain is drowned by calculating the fraction of its length that is below mean sea level due to sea level rise. Results show that barrier drowning is mostly sensitive to the wave height and the rate of sea level rise. In the model, it takes 100s of years for barrier islands to start drowning in response to high rates of sea level rise (more than 5 mm/yr, for a typical coastal environment). This lag in barrier response is caused by a gradual decrease in the sand volume of the barrier. Higher rates of sea level rise cause earlier and more severe barrier drowning. Modeled barrier systems that face higher waves undergo more frequent inlet closures that lower the rate of drowning, but they also have a deeper shoreface that increases the rate of drowning. In model simulations, the latter process dominates over the former when sea level rise rates exceed 5 mm/yr. Model results fairly agree with available field data.

Plain Language Summary In extreme sea level rise scenarios (like those predicted during the 21st century and beyond) barrier islands may drown. Barrier drowning occurs due to a lack of sediment induced by sea level rise, which causes submergence of (parts of) the barrier chain. It remains difficult to predict when and under which conditions drowning may occur. In this study we investigated the dynamics of drowning barrier islands with an exploratory numerical model. A key finding from our model is that high rates of sea level rise (higher than 5 mm/yr), but also high waves (higher than 1.5 m) result in barrier drowning. However, even under model simulations with high rates of sea level rise, it takes a long time for the sand in the barrier island to erode. Barrier drowning and disappearance therefore might take 100s of years. The model results are consistent with available field data, but more observations are needed to achieve a full model verification.

1. Introduction

Barrier islands are low-lying coastal land forms that constitute 10%–15% of the world's coasts (Davis & FitzGerald, 2010). They lie parallel to the mainland coast, thereby they protect it from coastal hazards such as storm surges (Davis & FitzGerald, 2010). As most coastal lowlands are densely populated, barrier islands are thus of great socio-economic importance.

Most barrier islands were created during the Holocene, when rates of relative sea level rise (RSLR) decreased from 7–15 to ~2 mm/yr (Beets & van der Spek, 2000; Leatherman, 1983). Different theories about barrier island formation have been proposed. Barriers may have formed through onshore migration of subtidal bars, or through the reworking of sediment after the continental shelf was flooded (Davis & FitzGerald, 2010). The latter mechanism is believed to be responsible for the formation of the Wadden Islands along the Dutch, German and Danish coast, some 7,000 years BP (Beets & van der Spek, 2000), as well as that of the barrier islands along the US east coast (Figure 1).

Future projected RSLR is a serious threat to most coastal systems in the world. Worst-case scenarios predict a global mean sea level (MSL) increase of roughly 2.7 m by the year 2300 compared to the year 2000 (Palmer et al., 2020). Furthermore, the effects of for example, vertical land motion should also be considered when studying the response of coastal systems to changes in sea level. Given that many barrier islands are located near deltas,

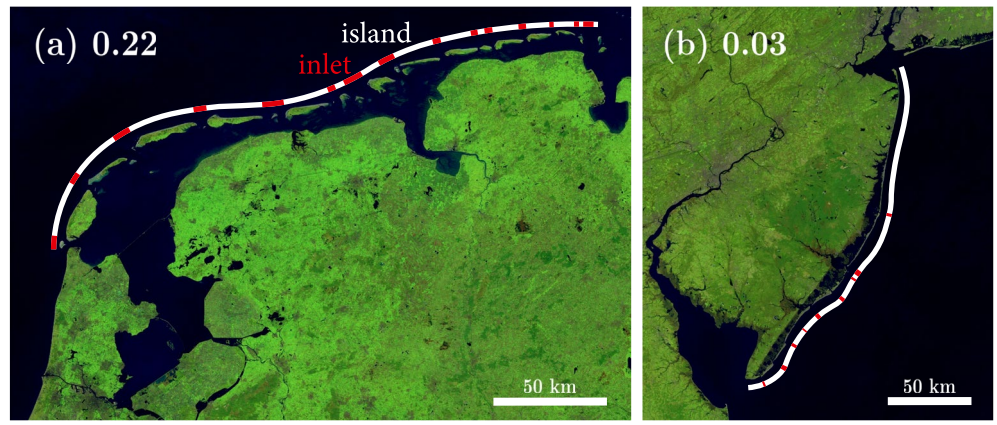

Figure 1. Relative sea level rise (RSLR) is expected to increase the fraction of barrier extent below mean sea level (MSL; Mellett & Plater, 2018). Examples of present-day barrier islands and their respective fraction below MSL (in the alongshore direction): (a) 0.22 for the Wadden Islands along the coasts of the Netherlands and Germany, and (b) 0.03 for the barrier islands along the US east coast of New Jersey. White curves represent the extent of islands, while red curves represent that of inlets. The given fraction below MSL is computed as the ratio between inlet width and the total barrier chain length (inlets and islands). Extracted from Google Earth (images provided by TerraMetrics).

where land is sinking, they may experience even higher rates of RSLR. Climate change may also result in changes in storm return periods, which also affect barrier coasts through changes in barrier breaching and sediment transport during overwash events (Reef et al., 2020).

A possible consequence of this increase in sea level, is that barrier islands will not be able to migrate landward fast enough to stay above sea level, resulting in whole-scale barrier island drowning (Mellett & Plater, 2018). Drowning, as we define it here in this study, is the submergence of (a part of) the barrier island chain due to sediment imbalance caused by RSLR. This includes whole-scale barrier drowning, in which the entire barrier chain is submerged below MSL, and also partial barrier drowning, in which part of the barrier chain is still above MSL and part of it is submerged. Partial barrier drowning could be a precursor to a whole-scale drowned barrier.

Observations of whole-scale drowned barrier systems are scarce. There is an example in the English Channel, where a barrier formed around 9,500–8,800 years BP, when MSL was at −22 m relative to that of present day, and it drowned around 8,300 years BP when MSL reached −17 m (Sanders & Kumar, 1975).

Observations of partial barrier drowning are more common. An example is the Isles Dernières barrier chain (Louisiana, USA), which has been exposed to a rate of RSLR of roughly 13 mm/yr since the mid-1800s (Dingler et al., 1993). As a response to this high rate of RSLR, new inlets have formed, and existing inlets have widened (FitzGerald et al., 2008). Other modern barrier island chains might also show signs of partial drowning, but this remains poorly quantified.

With high rates of RSLR, the part of a barrier island chain that is below MSL (inlets, see Figure 1) is expected to increase in the future (Mellett & Plater, 2018). Existing inlets might have been in equilibrium, due to a balance between sediment export by tidal currents and sediment import by littoral drift (Escoffier, 1940). But inlet sizes can increase because RSLR (when ignoring changes in ocean tides) causes an increase in tidal prism (Stage 2 of the conceptual model of FitzGerald et al., 2008). In addition, RSLR will create sediment deficits in the barrier chain that will further expand existing inlets beyond their equilibrium, and also create breaches that will form new inlets (Stage 3 of the conceptual model of FitzGerald et al., 2008). The threshold rates of RSLR that induce barrier island drowning are mostly unknown, and the subsequent drowning timescales could be of the order of 100s of years (Mariotti & Hein, 2022).

Here, we study the influence of RSLR on the long-term evolution (100s of years) of barrier island chains. In particular, we focus on the time needed for barrier islands to respond to changes in rates of RSLR, and on the key mechanisms that drive barrier island drowning.

Process-based models haven been commonly used to investigate barrier drowning. Stolper et al. (2005) developed the cross-shore Geomorphic Model of Barrier, Estuarine and Shoreface Translations (GEOMBEST) model,

21699011, 2023, 11, Downloaded from https://agupubs.onlinelibrary.wiley.com/doi/10.1029/2022JF007010 by University Of Twente Finance Department, Wiley Online Library on [06/11/2023]. See the Terms and Conditions (https://onlinelibrary.wiley.com/terms-and-conditions) on Wiley Online Library for rules of use; OA articles are governed by the applicable Creative Commons License

21699011, 2023, 11, Downloaded from https://agupubs.onlinelibrary.wiley.com/doi/10.1029/2022JF007010 by University Of Twente Finance Department, Wiley Online Library on [06/11/2023]. See the Terms and Conditions (https://onlinelibrary.wiley.com/terms-and-conditions) on Wiley Online Library for rules of use; OA articles are governed by the applicable Creative Commons License

which allows for the study of distinct stratigraphic units characterized by a different erodibility and sediment composition. Using the GEOMBEST model, Moore et al. (2010) showed the rate of RSLR to be the main factor determining barrier island drowning. Lorenzo-Trueba and Ashton (2014) designed a cross-shore model to study barrier island drowning and retreat due to RSLR. They found that a barrier drowns when landward sediment transport on the shoreface or across the islands is too small to maintain the barrier.

Cross-shore models can represent barrier drowning, but their findings are difficult to compare with observations. This is because they make a binary prediction (a barrier is either drowned or not) and most modern barrier chains will be somewhere in between. To study barrier island chains, two horizontal dimensions facilitate easier integration of models with observations. Such models have been recently developed (Ashton & Lorenzo-Trueba, 2018; Mariotti & Hein, 2022; Nienhuis & Lorenzo-Trueba, 2019). The model by Ashton and Lorenzo-Trueba (2018) follows the same parameterized cross-shore dynamics as that of Lorenzo-Trueba and Ashton (2014), and couples them in the alongshore direction by adding an equation for shoreline evolution that depends on alongshore variations of the shoreline. The BarrieR Inlet Environment (BRIE) model of Nienhuis and Lorenzo-Trueba (2019) accounts for inlet dynamics as well. Moreover, all these processes are included in the model of Mariotti and Hein (2022), which, in addition, also solves for hydrodynamics. The advantage of the highly parameterized BRIE model with respect to the more complex model of Mariotti and Hein (2022) is that it is fast, so it is a suitable tool for performing extensive sensitivity studies. Furthermore, since it explicitly accounts for inlet dynamics, such as opening, closing, or migration, it allows for simulating barrier island states that are in between fully emerged and fully drowned. However, BRIE only considers inlets that are in morphodynamic equilibrium (i.e., following Escoffier, 1940) and does not consider the dynamic effects of RSLR on inlets.

Motivated by the existing modeling restrictions, we modify and expand the BRIE model into the BarrieR Inlet Environment-Drowning (BRIE-D) model to allow for RSLR-driven transformations of tidal inlets on barrier island chains. Note that both BRIE and BRIE-D are "exploratory" models (Murray, 2003), aiming at understanding a poorly understood process (here, barrier drowning) rather than representing a specific barrier island.

Our study objectives are to (a) understand the effects of RSLR on the barrier island sediment balance, inlet expansion and the related barrier drowning, (b) examine the temporal evolution of inlet expansion in a drowning barrier, and (c) explore the dependence of barrier island drowning on model parameters (e.g., wave height, rate of RSLR, storm return period, tidal amplitude).

The next section includes a description on how barrier drowning is quantified and modeled, together with the design of simulations and analysis of model output. Section 3 contains the results, followed by a discussion in Section 4. The final section contains the conclusions.

2. Methods

2.1. Metrics for Studying Barrier Island Drowning

In this study, we use a measure for RSLR-driven barrier island drowning that is derived as follows. Consider a barrier island chain, with an alongshore extent L_b, separated by N different inlets, each having a width $W_{inlet,i}$, where $i = 1, 2, \ldots, N$. In the course of time, the number of inlets N may change as a result of islands becoming drowned, barrier storm breaching, inlet closure, and inlets merging. The width of each inlet may also change, and expand to become very wide with tips that are morphologically disconnected. We define the fraction of barrier extent that is drowned ΔF as

$$\Delta F = F - F_{eq},\ F = \frac{\sum_{i=1}^{N} W_{inlet,i}}{L_b},\ F_{eq} = \frac{\sum_{i=1}^{N} W_{inlet,eq,i}}{L_b}. \quad (1)$$

In this expression, F is the fraction of barrier extent below MSL (i.e., the part of L_b that consists of inlets, see e.g., Figure 1). However, F itself is not characterizing barrier drowning, as inlets do exist under non-drowning conditions. In the latter case, the inlets are said to be in equilibrium. The equilibrium widths of the inlets are denoted by $W_{inlet,eq,i}$, from which it follows the fraction F_{eq} of the barrier below MSL. As shown by Equation 1, it is the difference between F and F_{eq}, that is, the fraction ΔF of the barrier length below MSL due to tide-wave imbalance, that quantifies how much of a barrier is drowned.

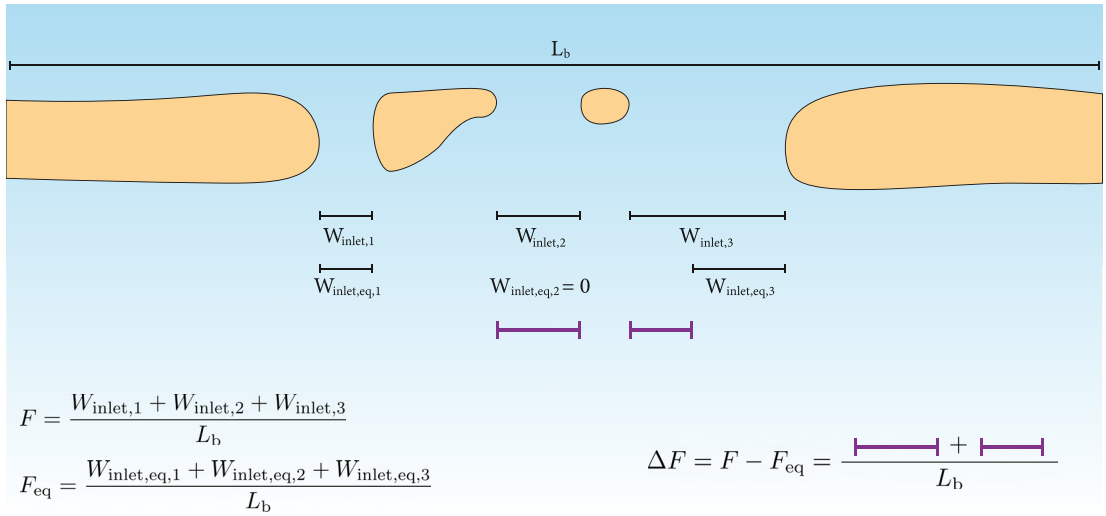

Figure 2. Graphical example of how the variables F, F_{eq}, and ΔF, which measure various aspects of drowning in our model, are defined. A chain (with total alongshore length L_b) of four barrier islands (yellow) and three inlets (widths $W_{inlet,1,2,3}$) is shown. In this case, Inlet 1 is in equilibrium ($W_{inlet,1} = W_{inlet,eq,1}$), Inlet 2 is fully drowned ($W_{inlet,eq,2} = 0$, i.e., according to equilibrium inlet theory it should be closed, but due to drowning of a portion of the barrier it is open), and the width of Inlet 3 consists of an equilibrium component and a drowned component. Purple segments represent the (parts of) inlet widths contributing to ΔF.

Note that a single inlet can be comprised of a part that is due to equilibrium, and another part due to drowning (see Figure 2 for a graphical example). The fraction of barrier extent that is drowned varies between 0 and 1. If $\Delta F = 0$, the barrier, on average, is in morphological equilibrium. Barrier drowning starts taking place when $\Delta F > 0$, which may precede a whole-scale drowned barrier.

Variations in F are caused by different mechanisms. Human modifications to barriers (constructing jetties, maintaining inlets, nourishments, etc.) cause deviations in the fraction of barrier extent below MSL. Short-term natural dynamics (storm breaching, inlet migration, etc.) also cause F to deviate away from its equilibrium. Here, we focus on RSLR, which affects ΔF but also F_{eq} through modifications of the tidal prism (FitzGerald et al., 2008). Section 2.3 describes how ΔF is computed from (BRIE-D model) data.

2.2. Model Description

We use the morphological BRIE-D model to study barrier drowning (measured with ΔF). We also use the BRIE model to simulate the evolution of a barrier chain that is always in equilibrium, thus not drowning. BRIE-D is an extension of the BRIE model (Nienhuis & Lorenzo-Trueba, 2019). The main differences between the two models are the following. In the original BRIE model, inlets are prescribed to have an equilibrium width ($F = F_{eq}$, such that $\Delta F = 0$). We modified BRIE into BRIE-D, in which a dynamic evolution of inlets is allowed that depends on the sediment mass balance. In this section, we describe inlet formation and evolution. Further details on the other model routines (e.g., cross-shore dynamics, shoreline evolution and numerical aspects) are given in Supplementary Information S1. More details about the BRIE model are given in Nienhuis and Lorenzo-Trueba (2019). In this paper, we compare BRIE-D to BRIE to investigate the effect of inlet dynamics on barrier drowning, and we use BRIE-D to then investigate barrier island drowning timescales. All results are from the (newer) BRIE-D, unless specified.

2.2.1. Inlet Opening

The BRIE-D model considers a barrier-inlet system with a given alongshore extent L_b. Initially, there are no inlets, but they can appear in two different ways. Inlets may open either due to barrier breaching caused by a storm or due to barrier drowning. Breaching is imposed every T_{storm} years where the barrier volume is at a minimum, and at a location at least 5 km from existing inlets (Roos et al., 2013). The time T_{storm} is to be interpreted as a storm return period. The initial width of a breached inlet is set at 1 km.

21699011, 2023, 11, Downloaded from https://agupubs.onlinelibrary.wiley.com/doi/10.1029/2022JF007010 by University Of Twente Finance Department, Wiley Online Library on [06/11/2023]. See the Terms and Conditions (https://onlinelibrary.wiley.com/terms-and-conditions) on Wiley Online Library for rules of use; OA articles are governed by the applicable Creative Commons License

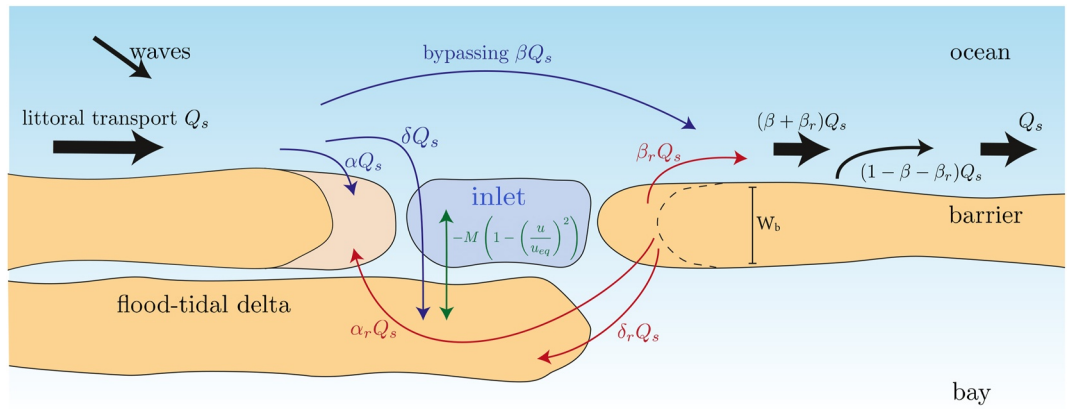

Figure 3. Sketch of the different elements of an inlet system and the mass exchanges with updrift and downdrift tips of the barrier, as well as with the flood-tidal delta. The parameters α, β, δ, α_r, β_r, and δ_r denote fractions of the littoral transport Q_s. Note that the flood-tidal delta extends through the updrift barrier because it has been building up as the inlet was migrating. Modified from Nienhuis and Lorenzo-Trueba (2019) and Nienhuis and Ashton (2016). A detailed description of the moving boundaries and the sediment exchange within the inlet is given in Supplementary Information S1.

Alternatively, inlets appear when a portion of the barrier drowns (either because the width or the height of the barrier becomes negative), which is not restricted to its proximity to other inlets. The initial width of a drowned inlet is set equal to the width of the portion of the barrier that drowned.

2.2.2. Inlet Evolution

Once inlets exist, the BRIE-D model calculates their widths and equilibrium widths (needed to calculate F, F_{eq}, and ΔF) as follows. First, inlet width W_{inlet} is related to cross-sectional area A_{inlet} by assuming a prismatic cross-section and a depth-to-width ratio (or aspect ratio) γ_{aspect}. The inlet aspect ratio is assumed to be constant only for small inlets. Based on observations (Hume & Herdendorf, 1992), the maximum inlet depth is set at 15 m, above which an increase in inlet cross-sectional area causes an increase in only the inlet width. Denoting the depth by D_{inlet}, it follows that $A_{inlet} = W_{inlet} D_{inlet} = \gamma_{aspect} W_{inlet}^2$, so

$$W_{inlet} = (A_{inlet}/\gamma_{aspect})^{1/2},\ W_{inlet,eq} = (A_{inlet,eq}/\gamma_{aspect})^{1/2}. \tag{2}$$

Now, $A_{inlet,eq}$ is calculated using the Escoffier (1940) relation, that is, from a balance between sediment import by waves and sediment export by tides (which depends on A_{inlet} and given tidal conditions). Details are given in Equations S61–S64 in Supplementary Information S1.

The evolution of the actual cross-sectional area A_{inlet} is governed by four drivers,

$$\frac{dA_{inlet}}{dt} = G_{sd} + G_{Esc} + G_m + G_d. \tag{3}$$

The first driver is G_{sd}, which represents the change in cross-sectional area resulting from the relative accretion and erosion of each inlet flank. As is shown in Figure 3, a fraction $\alpha + \alpha_r$ (depending on wave and tidal condition) of the alongshore wave-driven sediment transport Q_s is deposited on the tip of the updrift island, causing the updrift inlet flank to move at a rate dL_{up}/dt. Likewise, a certain fraction $\beta_r + \delta_r + \alpha_r$ of sediment is eroded from the downdrift inlet flank, causing it to move at a rate dL_{down}/dt. In the BRIE model, these deposition and erosion processes only result in migration of the inlet, and the value of δ_r is chosen such that inlet width is kept constant. In the BRIE-D model this constraint is released, resulting in variations in the cross-sectional area of the inlet, leading to

$$G_{sd} = D_{inlet}\left(\frac{dL_{down}}{dt} - \frac{dL_{up}}{dt}\right). \tag{4}$$

In the BRIE model this sediment distribution was such that the cross-sectional area of the inlet was maintained constant. In the BRIE-D model we allow for both tips of the barrier to be disconnected, and grow or shrink the

21699011, 2023, 11, Downloaded from https://agupubs.onlinelibrary.wiley.com/doi/10.1029/2022JF007010 by University Of Twente Finance Department, Wiley Online Library on [06/11/2023]. See the Terms and Conditions (https://onlinelibrary.wiley.com/terms-and-conditions) on Wiley Online Library for rules of use; OA articles are governed by the applicable Creative Commons License

21699011, 2023, 11, Downloaded from https://agupubs.onlinelibrary.wiley.com/doi/10.1029/2022JF007010 by University Of Twente Finance Department, Wiley Online Library on [06/11/2023]. See the Terms and Conditions (https://onlinelibrary.wiley.com/terms-and-conditions) on Wiley Online Library for rules of use; OA articles are governed by the applicable Creative Commons License

inlet. A description of the variations in updrift and downdrift sediment volumes is given in Equations S32–S40 in Supplementary Information S1.

We further allow for variations in the cross-sectional area of the inlet depending on the sediment exchange with the flood-tidal delta. This sediment exchange depends on a prescribed transport from the flood-tidal delta to the inlet and the export of sediment from the inlet to the flood-tidal delta due to tidal currents. For this, a simple model for an inlet-bay system is employed, as was used by Escoffier (1940) to explain the stability of tidal inlets. The changes on the cross-sectional area of the inlet governed by these dynamics are described by

$$G_{Esc} = -\frac{M}{W_b}\left(1 - \left(\frac{U}{U_e}\right)^2\right). \tag{5}$$

In this equation, W_b is the width of the barrier and U is the amplitude of the tidal current in the inlet (which depends on the imposed tidal amplitude at sea, the cross-sectional area of the inlet, the barrier width, and the wetted surface of the back-barrier lagoon). Furthermore, U_e is the amplitude of the tidal current at equilibrium (set at 1 m/s for all simulations), and M is the volume of sediment per time unit that the inlet receives from the flood tidal delta. With this representation of tidal dynamics we allow for the inlet to evolve toward an equilibrium configuration, using a parametrization of the net sediment transport due to tides that was earlier used by van de Kreeke (2004).

A third way inlets can increase their cross-sectional area is by merging with other inlets. The increase in the cross-sectional area of the inlet due to merging with other inlets G_m is such that the total cross-sectional area is conserved. As a result, if inlets j and k merge, with $j < k$, the cross-sectional area of inlet j is then $A_{inlet,j} + A_{inlet,k}$, and inlet k is no longer present at the next time step.

Lastly, the increase in the cross-sectional area of the inlet due to barrier drowning depends on the length W_d of the portion of the barrier that drowned (due to either a negative barrier width or a negative barrier height),

$$G_d = \frac{dW_d}{dt}\,\gamma_{aspect} W_d. \tag{6}$$

In the case of barrier drowning, it may be that, according to the inlet aspect ratio formulation, the inlet is deeper than the initial depth of the drowned portion of the barrier. In order to ensure sediment conservation, the sediment missing in the inlet is added to the flood-tidal delta.

2.3. Analysis of Model Output

We study the barrier response to RSLR through F, F_{eq}, and ΔF. Values for F, F_{eq}, and ΔF are computed from W_{inlet} and $W_{inlet,eq}$, which are output of the models. Note that the value of F_{eq} obtained with the BRIE-D model, which allows for a gradual evolution of inlets, will not be necessarily identical to the value of F obtained with the BRIE model, which imposes inlets to be in equilibrium. This is because the time evolution of both models is governed by different dynamics (Equation 3 in the BRIE-D model, allowing for a gradual evolution, vs. the immediate equilibrium imposed in the BRIE model). Indeed, the different processes implemented in the BRIE-D model interact with each other, resulting in non-linear dynamics. Thus, the number and distribution of inlets will be different in both models. This difference in number and distribution of inlets may lead to, for example, two inlets being closer in BRIE-D than in BRIE, producing different equilibrium inlet widths, and hence different values of F_{eq} in BRIE-D from the F in BRIE.

We study the timescales involved in barrier drowning by investigating the time series of ΔF under increasing rates of RSLR. Two timescales are defined: first, the time it takes until ΔF exceeds 0.1, and, second, the time it takes until ΔF exceeds 0.3. Here, the time at which $\Delta F = 0.1$ represents the moment at which a noticeable amount of drowning has occurred. The time at which $\Delta F = 0.3$ or, in other words, the situation where RSLR has submerged 30% of the barrier alongshore extent, represents the time at which an aggravated drowning has occurred and the barrier is even more prone to eventually fully drown.

We also study the time evolution of other morphological metrics of drowning barriers, namely the number of inlets and the barrier width. The latter is represented by its alongshore mean through time, and it is computed as

Table 1
Overview of Simulations Performed, Imposing Different Values for the Rate of Relative Sea Level Rise (RSLR) $(\dot{\xi})$ and Significant Wave Height (H_s)

Aim	Model used	Parameter range[a]	Figures
Effects of RSLR on inlet sediment balance	BRIE, BRIE-D[b]	$\dot{\xi} = 4, 17$ mm/yr	Figures 4 and 5
Temporal evolution of barrier drowning	BRIE-D	$\dot{\xi} = 4, 17$ mm/yr	Figure 6
Dependence on model parameters	BRIE-D	$\dot{\xi}$ varying between 2 and 20 mm/yr, H_s varying between 0.75 and 3 m[c]	Figures 7–9

[a]If not specified parameters take their default values (see Appendix A). [b]Same input parameters for both models. [c]Mulhern et al. (2017).

the distance between the seaward shoreline and the back-barrier shoreline. We compute the barrier width only along the parts corresponding to subaerial barrier, that is, where $W_b > 0$.

2.4. Design of Simulations

Our first aim is to understand the effects of RSLR on the barrier island sediment balance, inlet expansion and the related barrier drowning. We compare the evolution of a barrier system in which inlets are imposed to be in equilibrium to that of a barrier in which inlets dynamically evolve, depending on the sediment balance. We used the BRIE and BRIE-D models for each of these situations, respectively, both with the same input parameters. For the two situations, we further compare the evolution of the barrier for two rates of RSLR ($\dot{\xi} = 4, 17$ mm/yr) to represent a situation close to equilibrium, and a situation with drowning.

To achieve the second aim, that is, to examine the temporal evolution of inlet expansion in a drowning barrier, we performed simulations with the BRIE-D model for $\dot{\xi} = 17$ mm/yr. For the sake of comparison, we also include the situation that $\dot{\xi} = 4$ mm/yr (no drowning).

To achieve the third aim (quantify dependence of barrier island drowning on model parameters), we performed simulations with a broad range of significant wave heights, rate of RSLR, storm return period, wave period, wave asymmetry, inlet aspect ratio, maximum overwash transport, and the suspended sediment transport efficiency factor, which controls the shoreface transport. These are also performed with the BRIE-D model, in order to allow for a dynamic evolution of the inlets and study their effects on barrier drowning.

All simulations have a run time of 2,500 years, taking $\dot{\xi} = 2$ mm/yr during the first 2,000 years, which serves as model spin-up period. After model spin-up, when the system reaches a statistically stationary state in terms of inlet number and inlet migration rates, we change $\dot{\xi}$ in order to study the system response for another 500 years. All other parameters have values that are representative for a typical mid-latitude barrier island chain and are kept constant during the entire 2,500 years (see Appendix A for a full overview of the model parameters and their default values). The new $\dot{\xi}$ is not changed during the last 500 years of model evolution. Note that we do not aim to simulate any barrier system specifically, but to get a broad picture of barrier response to RSLR. Table 1 presents an overview of the simulations performed.

Since we deal with a stochastic system, where randomness originates from the wave angle and from the initial conditions (see Supplementary Information S1), we performed five model realizations for each parameter setting. We present the model results as the mean of the five realizations for each parameter setting. Errors are quantified using the standard error of the mean. Experiments performed with an ensemble size of 100 showed no significant differences in model outcome when compared to results computed with only five simulations.

3. Results

3.1. Effects of Dynamic Inlets on RSLR-Induced Barrier Drowning

An example BRIE-D model simulation allowing for dynamic inlets under a rate of RSLR $\dot{\xi} = 17$ mm/yr shows a gradual expansion of inlets during 500 years of barrier evolution (Figure 4). The barrier appears to drown gradually: initially (after the model spin-up period), the barrier is in a statistical equilibrium state. After 200 years drowning starts ($\Delta F = 0.2$), and after 400 years more than half of the alongshore extent of the barrier is below MSL ($\Delta F = 0.6$). The transition from a state in which inlets are in morphodynamic

21699011, 2023, 11, Downloaded from https://agupubs.onlinelibrary.wiley.com/doi/10.1029/2022JF007010 by University Of Twente Finance Department, Wiley Online Library on [06/11/2023]. See the Terms and Conditions (https://onlinelibrary.wiley.com/terms-and-conditions) on Wiley Online Library for rules of use; OA articles are governed by the applicable Creative Commons License

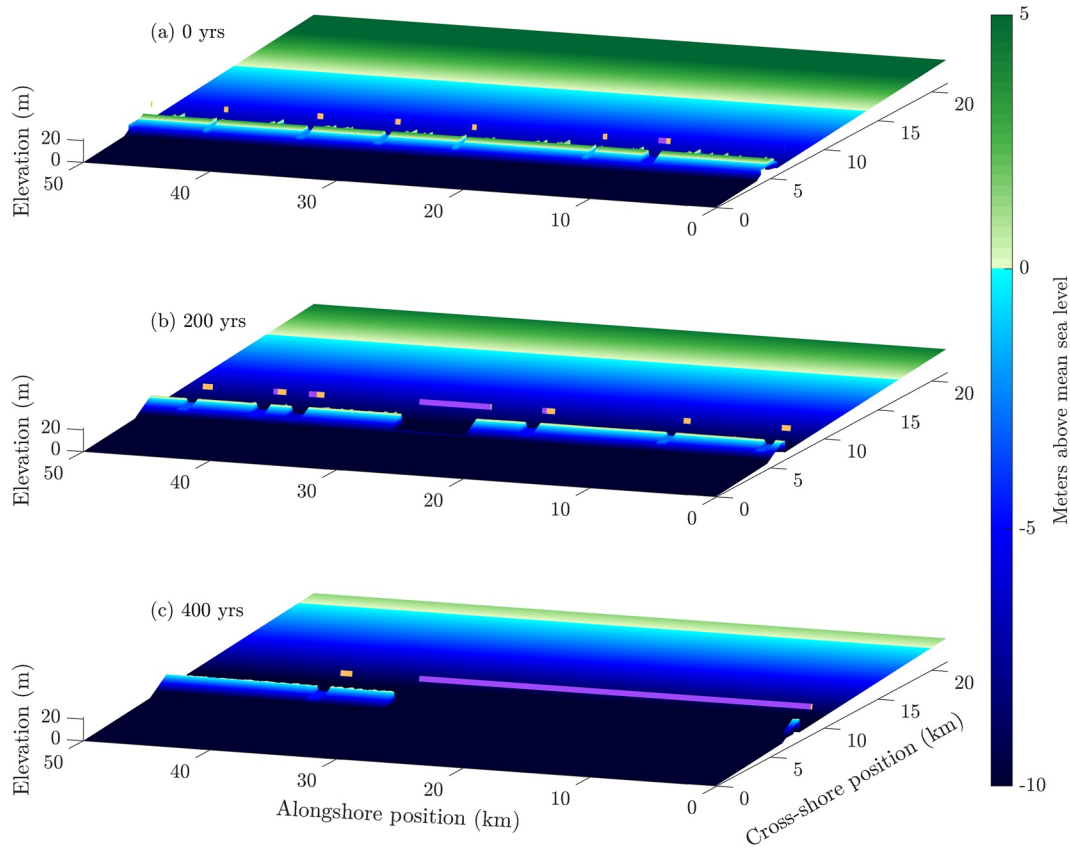

Figure 4. Modeled barrier island evolution (accounting for dynamic inlet evolution) at (a) 0, (b) 200, and (c) 400 years after the model spin-up period. Simulation is for a rate of relative sea level rise $\dot{\xi} = 17$ mm/yr and for a domain with an along-shore extent of 50 km. Orange lines represent the equilibrium width for each inlet ($W_{inlet,eq}$) and purple lines the difference between the actual inlet width an that at equilibrium. All parameters except $\dot{\xi}$ have their default values (see Table A1); in particular the offshore significant wave height is $H_s = 1.5$ m and the tidal amplitude is $a_0 = 0.8$ m.

equilibrium toward a state of drowning is evident after 200 years, as some inlets become much wider than in the equilibrium situation (~7 km). From there on, inlets merge and widen to the order of tens of km by the year 400.

In order to understand the potential effects of RSLR on inlet expansion and the related barrier drowning, we performed simulations allowing for a gradual evolution of inlets depending on the barrier sediment balance. We compare their output to that of simulations in which inlets are imposed to be in equilibrium. To study the effects of RSLR, we use low and high rates of RSLR ($\dot{\xi} = 4$ and $\dot{\xi} = 17$ mm/yr, respectively). Recall that for all simulations a spin-up period of 2,000 years with $\dot{\xi} = 2$ mm/yr is used.

For low $\dot{\xi}$, there are differences in barrier evolution between the situation in which inlets are imposed to be in equilibrium and the situation in which they are allowed to gradually evolve (Figures 5a and 5b), albeit that no drowning occurs in this case. Inlets tend to close more easily when they can gradually evolve in time (Figure 5a). This is because they are allowed to be closer to the "unstable equilibrium" (Equation 5, Escoffier, 1940), when inlet narrowing starts to decrease inlet flow velocities below the equilibrium velocity. In addition, independent updrift and downdrift flank migration rates (Equation 4) will also cause a greater instability in inlet size, which could lead to more frequent closure (as well as inlets larger than the stable equilibrium). Nevertheless, on longer timescales, low RSLR rates also lead to relatively steady inlet widths over time, similar to model simulations with the equilibrium imposed (Figure 5b). Furthermore, inlet migration rates are generally similar in both situations (~1 to 2 m/yr), with the exception of short periods in which dynamic inlets migrate at rates of order 200 m/yr, due to local narrowing of the barrier. These low rates of RSLR do not present signs of an adaptation period to the new value of $\dot{\xi}$ imposed at $t = 0$.

21699011, 2023, 11, Downloaded from https://agupubs.onlinelibrary.wiley.com/doi/10.1029/2022JF007010 by University Of Twente Finance Department, Wiley Online Library on [06/11/2023]. See the Terms and Conditions (https://onlinelibrary.wiley.com/terms-and-conditions) on Wiley Online Library for rules of use; OA articles are governed by the applicable Creative Commons License

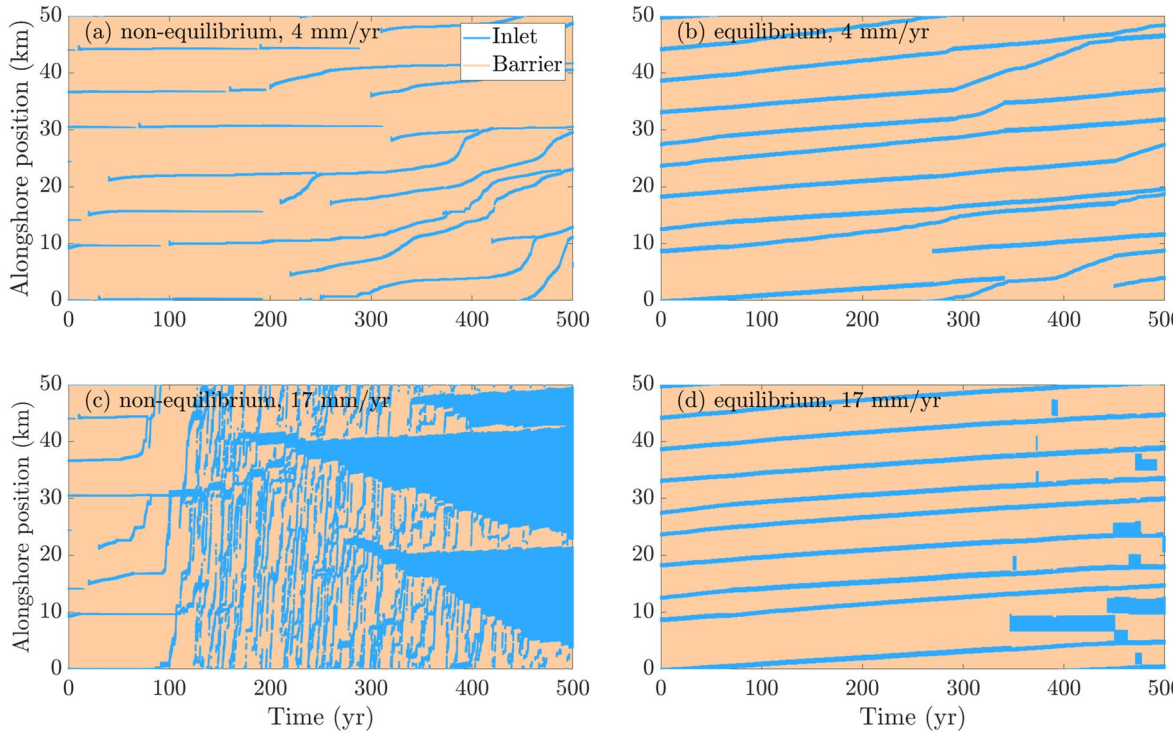

Figure 5. Comparison between the output of a model that allows for a gradual evolution of the cross-sectional area of the inlets (BRIE-D), and that of a model imposing inlets to be in equilibrium (BRIE): temporal evolution of barrier systems during 500 years in a 50 km long domain for a $\dot{\xi}$ of (a and b) 4 mm/yr (barrier drowning is not occurring) and (c and d) 17 mm/yr (there is barrier drowning causing widening the inlets). Simulations (a and c) allow for a gradual evolution of the inlets, whilst in simulations (b and d) inlets attain equilibrium instantaneously. All parameters except $\dot{\xi}$ have their default values (see Table A1); in particular the offshore significant wave height is $H_s = 1.5$ m and the tidal amplitude is $a_0 = 0.8$ m.

Simulations under high rates of RSLR ($\dot{\xi} = 17$ mm/yr) reveal that when inlets are imposed to be in equilibrium, the response of the system strongly differs from that in which inlets can gradually evolve (Figures 5c and 5d). In general, imposing equilibrium yields an irregular evolution of inlet widths, with abrupt changes taking place for example, at the years 450 and 465, or with inlet closing briefly after opening at years 350–400. This behavior is due to barrier drowning being disconnected from (other) inlet dynamics. In contrast, by allowing for feedbacks between tide-induced inlets and drowning-induced inlets, we see more gradual inlet evolution. The resulting barrier behavior is smoother, but also a faster increase in ΔF is seen. Another difference between the non-equilibrium (BRIE-D, Figure 5c) and equilibrium (BRIE, Figure 5d) inlet model for $\dot{\xi} = 17$ mm/yr is the resulting inlet migration rate. The non-equilibrium model yields higher migration rates (~5 km/yr) compared to the equilibrium model (~10 m/yr) for narrow inlets (<2 km). These high migration rates appear when the barrier is very narrow (<100 m). The difference between the two models is caused by the updrift and downdrift barrier tips evolving independently (G_{sd}, Equation 4), imposed to allow for inlet widening beyond its equilibrium state. This disconnection causes differences in sediment deposition in the inlet, which alters inlet migration. Note the time lag in barrier response in the BRIE-D model after the rate of RSLR has increased from 2 to 17 mm/yr at $t = 0$. It takes 100–150 years for the barrier to adapt to the new conditions.

3.2. Evolution of a Drowning Barrier

Allowing for non-equilibrium inlets in a drowning barrier affects the temporal evolution of F, ΔF, F_{eq}, barrier width W_b and the number of inlets (Figure 6). In the case of dynamic inlets and a high rate of RSLR ($\dot{\xi} = 17$ mm/yr), Figure 6a shows that F gradually increases from the year 100 up to ~0.8 after 500 years. When inlet equilibrium is imposed, F also increases, due to an increase in tidal prism, reaching values up to 0.3. This increase in F corresponds to the sudden inlet creation and inlet widening taking place from the year 350 onward (see Figure 5e). Gradually evolving inlets result in a gradually increasing F from the year ~100. The situation with a low rate of RSLR ($\dot{\xi} = 4$ mm/yr) shows a constant F for both situations.

21699011, 2023, 11, Downloaded from https://agupubs.onlinelibrary.wiley.com/doi/10.1029/2022JF007010 by University Of Twente Finance Department, Wiley Online Library on [06/11/2023]. See the Terms and Conditions (https://onlinelibrary.wiley.com/terms-and-conditions) on Wiley Online Library for rules of use; OA articles are governed by the applicable Creative Commons License

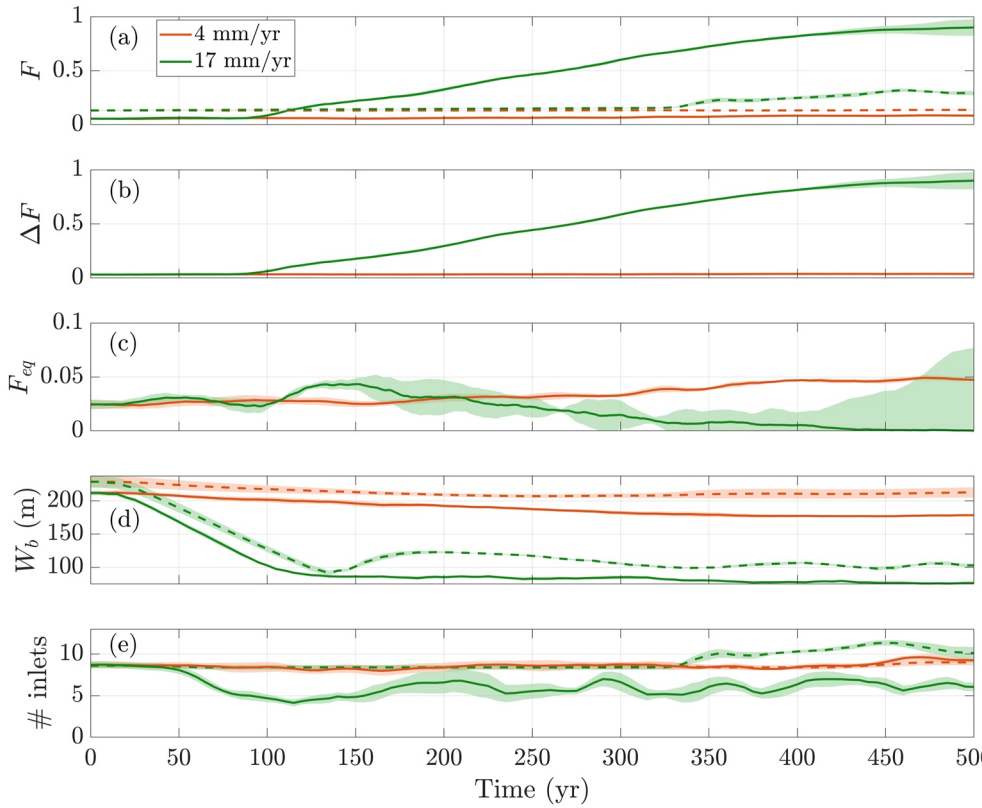

Figure 6. (a) Time series of F for $\dot{\xi} = 4$ and $\dot{\xi} = 17$ mm/yr, comparing barrier drowning under non-equilibrium inlet dynamics (solid) and equilibrium inlet dynamics (dashed). Panel (b) as panel (a), but for ΔF (only for non-equilibrium inlet dynamics because $\Delta F = 0$ for inlets in equilibrium). Panel (c) as panel (b), but for F_{eq}. Panel (d) as panel (a), but for mean barrier width W_b. Panel (e) as panel (a), but for the number of inlets. Curves represent the mean over five simulations. Shaded areas represent the standard error of the mean. Note the different scales of the vertical axes.

When allowing for dynamic inlets, ΔF is much larger than F_{eq} for $\dot{\xi} = 17$ mm/yr (see Figures 6b and 6c), meaning that drowning is the main process through which inlets are created and maintained open. The fraction ΔF starts to deviate from zero after 100 years of evolution when $\dot{\xi} = 17$ mm/yr, and achieves a value of 0.8 after 400 years more. In contrast, the simulation during which $\dot{\xi} = 4$ mm/yr is always close to equilibrium, that is, ΔF is always close to zero with a maximum deviation of 0.001. In this situation of low rate of RSLR, the barrier moves landward without losing mass or subaerial surface area. Accordingly, ΔF remains constant. This means that landward migration of the barrier sufficiently offsets lagoon widening to prevent severe changes in the tidal prism and thus drowning from increases in tidal prism does not occur. This is consistent with observations from Deaton et al. (2017).

The fraction F_{eq} decreases until reaching a value of 0 after 500 years of evolution for $\dot{\xi} = 17$ mm/yr. This is because F_{eq} is a metric arising from each individual inlet (not the barrier chain as a whole), thus it decreases when the barrier starts to drown and inlets starts to merge. With $\dot{\xi} = 4$ mm/yr, F_{eq} slightly increases from 0.025 to 0.05 because of a small increase in tidal prism caused by lagoon widening.

Barrier width rapidly decreases in the simulations with $\dot{\xi} = 17$ mm/yr during the first ~100 to 150 years of evolution after spin-up (see Figure 6d). This means that the sediment reservoir of the barrier (its sediment volume) starts decreasing briefly (less than 30 years) after the barrier is exposed to a new rate of RSLR. This period is a transition period, in which the barrier is adjusting to the new $\dot{\xi}$. There is also a minor decrease in barrier width for the case $\dot{\xi} = 4$ mm/yr, regardless of the inlets being always close to equilibrium. The barrier width eventually reaches an equilibrium value that depends on the $\dot{\xi}$ imposed. That value is about 30 m larger when imposing inlet equilibrium instead of allowing for a gradual inlet evolution for the two values of $\dot{\xi}$ shown. This difference is due

21699011, 2023, 11, Downloaded from https://agupubs.onlinelibrary.wiley.com/doi/10.1029/2022JF007010 by University Of Twente Finance Department, Wiley Online Library on [06/11/2023]. See the Terms and Conditions (https://onlinelibrary.wiley.com/terms-and-conditions) on Wiley Online Library for rules of use; OA articles are governed by the applicable Creative Commons License

to the added inlet dynamics in the latter situation. Adding sediment exchange between the inlet and the flood-tidal delta decreases sediment availability along the barrier islands, thereby reducing the barrier width.

Both configurations, that is, equilibrium and non-equilibrium inlet dynamics, produce roughly the same number of inlets for $\dot{\xi} = 4$ mm/yr (Figure 6e), because the inlets are close to equilibrium (i.e., $\Delta F \sim 0$). In equilibrium, the number of inlets is controlled solely by the available tidal prism and the alongshore distance at which inlets remain stable (Roos et al., 2013). Thus, the number of inlets remains constant at ~8 to 9. For faster RSLR ($\dot{\xi} = 17$ mm/yr), equilibrium and non-equilibrium inlets start to behave differently. The number of inlets fluctuates between 8 and 9 when imposing equilibrium, showing no big differences with the situation with lower $\dot{\xi}$ until the year 350. After 350 years, it increases up to ~11 to 12. In contrast, when letting inlets gradually evolve in time, the number of inlets decreases to ~5 to 6 and fluctuates around these numbers from the year ~200 onward. This is because inlets are wider when they are not restricted to be in equilibrium, thus there is less subaerial portion of the barrier where inlets may form and survive without merging with other existing inlets.

3.3. Wave Height and RSLR Effects on Barrier Drowning

We performed a sensitivity analysis for the main parameters that control the system: tidal amplitude, significant wave height, wave period, rate of RSLR, wave asymmetry, inlet aspect ratio, storm return period, maximum overwash transport and the suspended sediment transport efficiency factor, which controls the shoreface transport. The significant wave height H_s and the rate of RSLR $\dot{\xi}$ turned out to be the parameters with the strongest impact on barrier drowning. The full sensitivity analysis is presented in Appendix B.

The fraction of barrier extent below MSL, F, changes due to the variations in F_{eq}, and in ΔF. Here, F_{eq} shows a dependence on significant wave height H_s and rate of RSLR $\dot{\xi}$ (see Figure 7a). This dependence is mainly caused by variations in tidal prism and sediment imported into the inlets by the littoral drift. For example, higher waves cause a decrease in F_{eq}, because they tend to close existing inlets. Nevertheless, variations in F_{eq} are low compared to the effects of drowning (see Figure 7b). There are two mechanisms that explain why ΔF shows more variations than F_{eq}. First, RSLR results in thinner barriers, decreasing barrier volume, and thereby higher G_{sd}. Second, waves affect shoreface sediment transports, increasing the potential onshore sediment transport, but also the shoreface depth (see Supplementary Information S1), leading to higher ΔF for intermediate wave height. The behavior of F is only dominated by that F_{eq} for low rates of RSLR ($\dot{\xi} < 5$ mm/yr), where the effect of RSLR is lower (see Figure 7c).

Overall, the results of Figure 8 reveal that an increase in $\dot{\xi}$ causes more drowning, as ΔF eventually takes larger values (see Figures 8a1, 8b1, and 8c1). ΔF, deviates from zero for rates of RSLR larger than a certain threshold ($\dot{\xi} \sim 6$ mm/yr). For $\dot{\xi}$ lower than 6 mm/yr, maximum differences in ΔF are 0.04 by the year 500. A similar general dependency of the barrier width W_b on the rate of RSLR is seen (Figures 8a2, 8b2, and 8c2), which attains lower values at latter times and at higher $\dot{\xi}$. Yet, W_b responds earlier to changes in $\dot{\xi}$, presenting more variability with respect to the initial value than ΔF after $t = 100$ years. Note that these values depend on other parameters as well (e.g., tidal amplitude, maximum overwash transport).

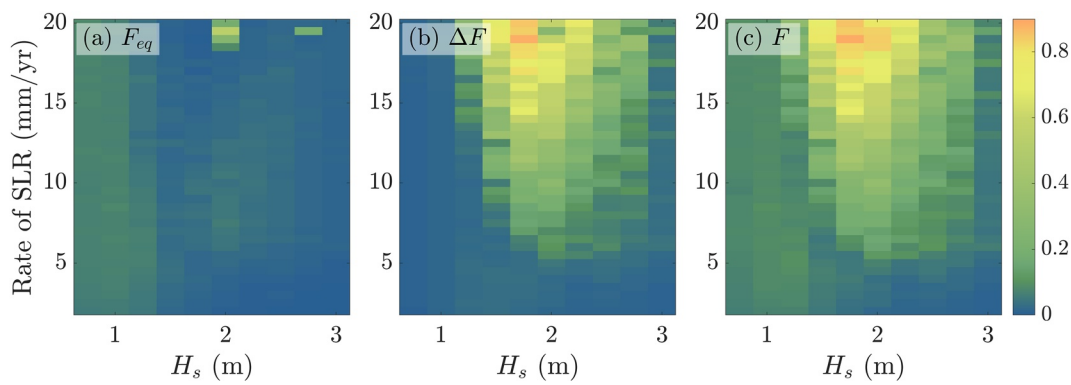

Figure 7. For different values of significant wave height H_s and rate of relative sea level rise $\dot{\xi}$: (a) the fraction of barrier extent below mean sea level (MSL), assuming an equilibrium situation for the inlets (F_{eq}), (b) the fraction of barrier extent below MSL due to tide-wave imbalance in the inlet (ΔF), and (c) the fraction of barrier extent below MSL ($F_{eq} + \Delta F = F$) at the year 300.

21699011, 2023, 11, Downloaded from https://agupubs.onlinelibrary.wiley.com/doi/10.1029/2022JF007010 by University Of Twente Finance Department, Wiley Online Library on [06/11/2023]. See the Terms and Conditions (https://onlinelibrary.wiley.com/terms-and-conditions) on Wiley Online Library for rules of use; OA articles are governed by the applicable Creative Commons License

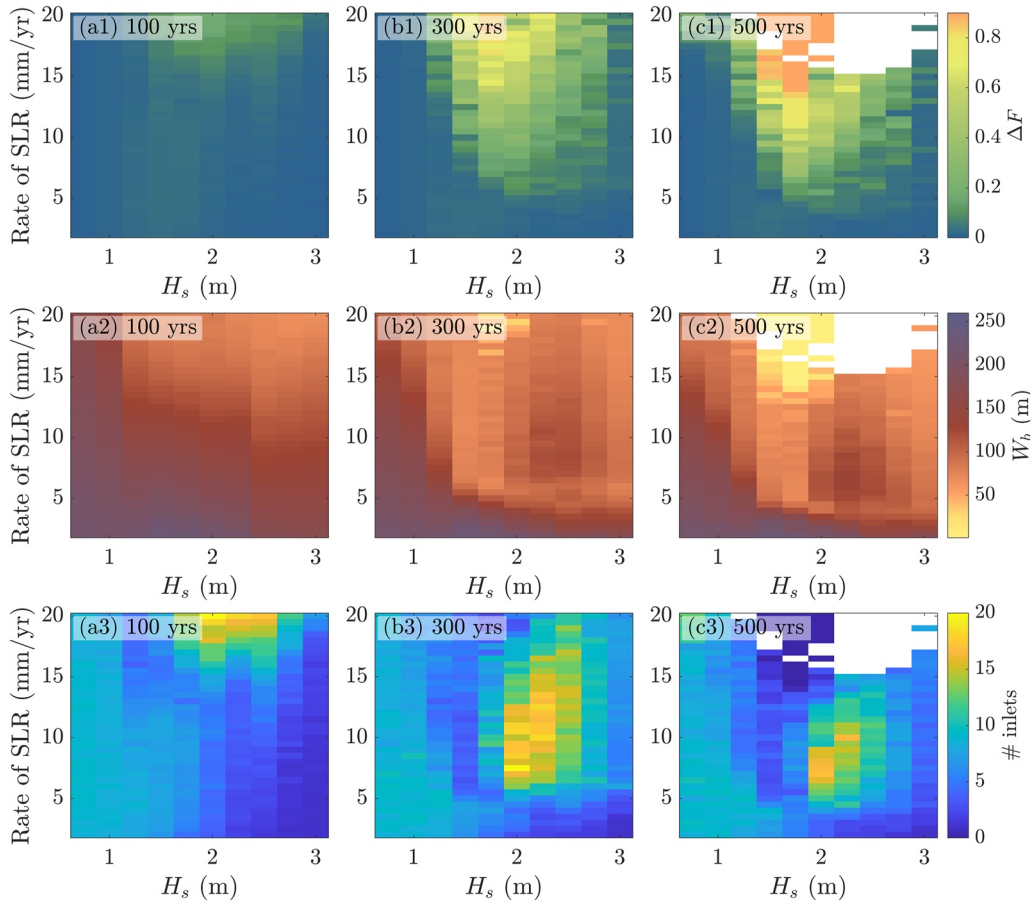

Figure 8. For different values of significant wave height H_s and rate of relative sea level rise $\dot{\xi}$: color plots of ΔF (a1, b1, c1), alongshore mean of barrier width W_b (a2, b2, c2), and number of inlets (a3, b3, c3). All three quantities are shown at years 100, 300 and 500 after model spin-up (first, second, and third columns, respectively) and averaged over five simulations. Situations depicted in white in panels (c1–c3) correspond to simulations that became numerically unstable while inlets were widening due to barrier drowning and thus stopped before reaching the year 500. Other simulations yielded a fully drowned barrier, represented by $\Delta F = 0.9$, $W_b = 0$, and no inlets (top central part of panels (c1–c3)).

The number of inlets does not show such a clear dependence on H_s and $\dot{\xi}$ as ΔF or W_b (see Figures 8a3, 8b3, and 8c3). Specifically, there are some cases with RSLR-driven drowning with a low number of inlets with (some of) them being very wide (W_{inlet} ~10 to 20 km). In other cases with barrier drowning, widths of inlets overall take lower values (W_{inlet} ~1 to 5 km). Still, the total fraction below MSL is larger than that at equilibrium, because the number of inlets is very large (~15 to 20). Situations in which there is barrier drowning with a large number of relatively narrow inlets are characterized by high waves ($H_s \geq 2$ m) and rates of RSLR generally lower than 15 mm/yr. In these situations, there is an important deposition of sediment by the littoral drift, which creates narrower inlets. In contrast, drowning situations with few and wide inlets only take place for $\dot{\xi} > 15$ mm/yr and intermediate H_s. In these cases, the combined effect of the deepening of the toe of the shoreface (see Equation S1 in Supplementary Information S1) and RSLR causes a widening of the inlets which can not be balanced by the sediment import of waves. Thus, simulations with similar ΔF and W_b may have a significantly different number of inlets.

Depending on the rate of RSLR and on the wave height, the barrier starts drowning (if it does) after a certain time. In all cases, this is not achieved instantly after the rate of RSLR changes, but there is a time lag for the barrier system to adapt. Situations in which ΔF attains a value of 0.1 or 0.3 are reached earlier for environments with higher $\dot{\xi}$ and intermediate H_s (Figure 9). The time lag depends on $\dot{\xi}$ because of the gradual evolution of the inlets cross-sectional area. Still, for the same rate of RSLR, this lag in barrier response depends on H_s as well, with

21699011, 2023, 11, Downloaded from https://agupubs.onlinelibrary.wiley.com/doi/10.1029/2022JF007010 by University Of Twente Finance Department, Wiley Online Library on [06/11/2023]. See the Terms and Conditions (https://onlinelibrary.wiley.com/terms-and-conditions) on Wiley Online Library for rules of use; OA articles are governed by the applicable Creative Commons License

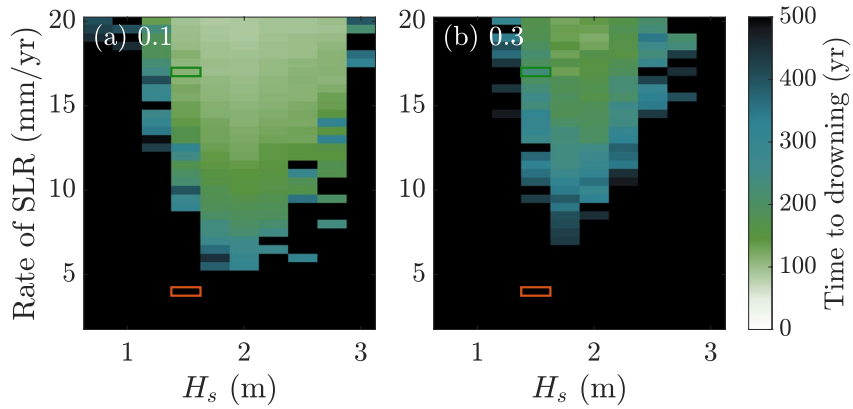

Figure 9. Color plots of drowning timescales (time after spin-up needed to reach (a) $\Delta F = 0.1$ or to reach (b) $\Delta F = 0.3$) for different significant wave heights H_s and rate of relative sea level rise $\dot{\xi}$. Green and red rectangles refer to the situations shown in Figure 6.

intermediate wave heights (H_s ~2 m) yielding the fastest barrier response. Intermediate H_s causes more drowning due to the deepening of the shoreface toe, which cannot be counteracted by the increased import of sediment into the inlets by the littoral drift. A deepening of the shoreface toe means a larger volume of sand that has to adapt to RSLR, thus creating more prone to drowning barriers. For higher waves, sediment imported by the littoral drift is able to counteract the effects of the deepening of the shoreface toe, and it takes longer for a barrier to drown. For lower waves, even if the sediment imported by the littoral drift is not so abundant, the toe of the shoreface is shallower, thus the whole barrier system adapts faster to RSLR-induced drowning. Interestingly, even if most situations deviate from equilibrium, not all of them reach a state that is characterized by $\Delta F = 0.1$ within 500 years.

Most model simulations of barrier drowning are numerically robust for both BRIE and BRIE-D. All quantities shown in Figures 7–9 have a low standard error compared to their mean. For ΔF, this value takes generally values below 0.05 and only reaches 0.15 in situations where ΔF is of the order of 0.9. The standard deviation of the mean barrier width is always below 15 m, and generally around 5 m. Lastly, the standard deviation of the mean number of inlets is always below 3. Only after 500 years of evolution and high rates of RSLR ($\dot{\xi} > 15$ mm/yr) and wave heights ($H_S > 2$ m) some of the simulations become numerically unstable during barrier drowning (white patches in Figure 8). We further explored the sensitivity of model output to halving the grid size and halving the time step and found that differences in F and ΔF were smaller than 3% for the situation with default parameter values.

4. Discussion

4.1. Choice of Parameters

The main objective of this study was to gain insight on the different dynamics related to barrier drowning. For simplicity, we have kept wave height, tidal amplitude and storm return period constant through the simulations, albeit they are expected to change as $\dot{\xi}$ increases (Bricheno & Wolf, 2018; Pickering et al., 2012). The chosen values are representative of different barrier systems in the world (Mulhern et al., 2017).

Our RSLR scenarios may not be representative of all barrier systems. We have chosen a spin-up period with $\dot{\xi} = 2$ mm/yr, followed by 500 years with a constant $\dot{\xi}$ between 2 and 20 mm/yr through all simulations, which allows for a broader range of scenarios. A constant $\dot{\xi}$ causes an abrupt change in the system after model spin-up, inducing an adaptation period of ~100 years (see Figures 5 and 6). The irregularities in the backbarrier shoreline just after spin-up (see Figure 4a) may be another manifestation of the abrupt change in $\dot{\xi}$. Still, these irregularities are smoothed with time and end up disappearing, hence we do not consider them to be a sign of model instability.

Additional simulations with accelerating rates of RSLR (based on RCP scenarios) showed the same tendency as the respective simulations with equivalent constant rates of RSLR (see Figure S8 in Supplementary Information S1). Future studies could, however, study in further detail the effects of a gradual increase in rate of RSLR by varying the increase in sea level as well as the timescale involved in this gradual evolution. Furthermore, variations in storm return period did not cause substantial differences on the results (see Appendix B).

21699011, 2023, 11, Downloaded from https://agupubs.onlinelibrary.wiley.com/doi/10.1029/2022JF007010 by University Of Twente Finance Department, Wiley Online Library on [06/11/2023]. See the Terms and Conditions (https://onlinelibrary.wiley.com/terms-and-conditions) on Wiley Online Library for rules of use; OA articles are governed by the applicable Creative Commons License

21699011, 2023, 11, Downloaded from https://agupubs.onlinelibrary.wiley.com/doi/10.1029/2022JF007010 by University Of Twente Finance Department, Wiley Online Library on [06/11/2023]. See the Terms and Conditions (https://onlinelibrary.wiley.com/terms-and-conditions) on Wiley Online Library for rules of use; OA articles are governed by the applicable Creative Commons License

4.2. Comparison With Earlier Models

The cross-shore dynamics reproduced by gradually evolving inlets (BRIE-D model) are similar to those obtained with the BRIE model of Nienhuis and Lorenzo-Trueba (2019) and with an earlier 2D horizontal barrier island model (which did not include inlets) of Lorenzo-Trueba and Ashton (2014). Barrier width eventually attains a constant value that depends on $\dot{\xi}$. Lorenzo-Trueba and Ashton (2014) found the same behavior and termed this state as dynamic equilibrium, because the barrier is still migrating landward, but its width does not change. Similarly, the more severe barrier drowning found for larger wave heights due to a deepening of the toe of the shoreface is in agreement with results of Lorenzo-Trueba and Ashton (2014). Differences include the barrier susceptibility to RSLR, which can be lower in BRIE and BRIE-D, because these also account for additional landward sediment transports due to inlet and alongshore dynamics.

Compared to BRIE, the BRIE-D model computes very high inlet migration rates for higher $\dot{\xi}$ (~5 km/yr, see Figure 5c). These rates mostly appear for narrow barriers under high rates of RSLR. BRIE-D inlet migration rates exceed rates commonly found along modern barrier islands, as indicated by a compilation of Nienhuis and Ashton (2016), who found a maximum of 700 m/yr. The BRIE model yields more realistic migration rates (of the order of 10 m/yr, see Figure 5d). These differences are caused by different migration speeds of the updrift and downdrift tips of the barrier, which allow for inlet widening. They may also result in unrealistically large inlet migration rates. Inlet dynamics in BRIE-D are based on Delft3D simulations from Nienhuis and Ashton (2016), who computed the distribution of sediment transport between the updrift and downdrift tips of the barrier. However, their experiments were performed with barrier widths between 250 and 800 m and inlets narrower than 1 km. Thus, situations with RSLR-driven drowning were not included. Future studies should investigate how to better parameterize inlet sediment distributions under drowning situations in which the barrier becomes narrower, possibly inducing new inlet dynamics. Inlet expansion rather than inlet migration is a key mechanism for barrier drowning. Yet, lower inlet migration rates would result in a more realistic overall barrier behavior. There would be less frequent inlet merging, which would leave less space available for barrier breaching, and would result in narrower inlets. Given that changes in inlet cross-sectional area of wider inlets only affect inlet width (not depth), having narrower inlets would result in lower F, and probably lower ΔF. Given that barrier width shows the same dependencies on wave height and rate of RSLR as ΔF, we expect the broad picture to be the same even with more realistic inlet migration rates.

The observed lag in barrier drowning (ΔF) to the abrupt change in rate of RSLR at $t = 0$ is of the order of ~100 to 300 years for $\dot{\xi} = 5 - 20$ mm/yr. Mariotti and Hein (2022) found barrier retreat lags changes in $\dot{\xi}$ by 500 years for $\dot{\xi} = 1 - 10$ mm/yr. They explained this lag by the presence of a barrier "geomorphic capital"; that is, the rate of landward retreat increases only after the sediment reservoir of the barrier has decreased enough, and the barrier has adjusted to the new $\dot{\xi}$. The BRIE-D model results represent this mechanism as well. The barrier width, as an indicator for its sediment reservoir, decreases first. Drowning starts when the barrier width has decreased and the littoral sediment transport into the inlets can no longer keep up with RSLR. Thus, the barrier first looses part of its sediment reservoir, and then starts drowning (increases in ΔF after several 100s of years, Figure 9).

4.3. Comparison With Observations

The scant observations that exist on barrier drowning are comparable to our simulations. The Isles Dernières have experienced gradual drowning during the last ~200 years under a rate of RSLR of 13 mm/yr (Dingler et al., 1993). For this barrier island chain, F increased from 0.05 to 0.37 to 0.55, in the years 1853, 1934, and 2015, respectively (obtained from aerial images provided in Davis and FitzGerald (2010)). Simulations performed with the BRIE-D model with a rate of RSLR of 13 mm/yr resulted in a similar behavior. Starting from $F = 0.06$ after 100 years after model spin-up (such that the model has adapted to the new $\dot{\xi}$), F increases up to 0.3 after 80 years of evolution, and to 0.45 after another 80 years (see Figure 10). But, situations might not be perfectly comparable. Part of the Isles Dernières barrier drowning could have been the result of marsh loss (FitzGerald et al., 2008; Lorenzo-Trueba & Mariotti, 2017) instead of sedimentary deficits. BRIE-D does not simulate marsh loss and its influence on the tidal prism, so more research, and perhaps model updates, are needed to further investigate the causes of Isles Dernières barrier drowning. In addition, model outcomes are also sensitive to other factors (e.g., shoreface response rate, maximum overwash transports) that are difficult to retrieve from field

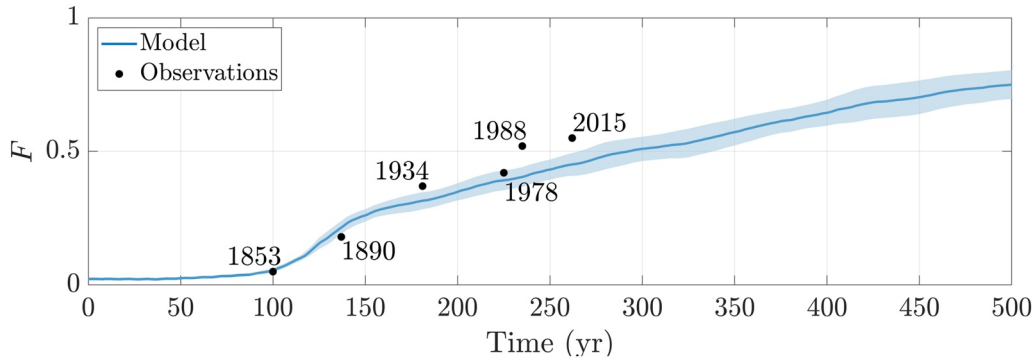

Figure 10. Time series of F for $\dot{\xi} = 13$ mm/yr, and observations of F for the Isles Dernières (obtained from aerial images provided in Davis and FitzGerald (2010)). We align the year 1853 with the model year 100 after spin-up to account for the time needed for the modeled barrier to adapt to the new $\dot{\xi}$.

observations. Nevertheless, the gradual disintegration of a barrier subject to RSLR and timescales involved are qualitatively similar.

Another way to compare our BRIE-D model simulations to observations is to consider F, the fraction below MSL. For example, the Wadden Islands have an F of 0.22, and the New Jersey coast has an F of 0.03 (Figure 1). The time evolution of F could be obtained from satellite images (Figure 1), available since the 1980s, as well as historic maps that go back further. Future work could be designed to model the evolution of barrier casts and calibrate and/or validate based on observed F, and then separate between ΔF and F_{eq} to study potentially ongoing, or future drowning.

4.4. Limitations in Modeling and Analysis

The BRIE-D model is not able to reproduce all the dynamics involved in barrier drowning. For example, we have not modeled the curvature of barrier tips occurring in wide inlets when bypassing diminishes (Davis & FitzGerald, 2010). Future research should focus on finding appropriate parametrizations for these dynamics and implementing them in the BRIE-D model such that the drowning state of a barrier is modeled as realistically as possible.

Note that the BRIE-D model includes a "storm" component, during which breaching occurs (by imposing a new inlet). It would be interesting to make the model more stochastic, and to link the occurrence and effects of storms to the offshore wave conditions that now only affect long-shore and cross-shore transport. A possible approach to do this is to assess what the correct scaling is to reduce the effects of stochastic wave heights into a single parameter (similar to geomorphic flood for river discharge). Ortiz and Ashton (2016) did this for cross-shore transport, but we are not aware of similar scaling rules for overwash or other critical processes. It would be interesting to investigate this in future studies.

Furthermore, the ebb-tidal delta is not explicitly included in the BRIE-D model albeit it is a prominent entity in the sand balance of tidal inlets. Nevertheless, its effects on inlet migration rate and the size of the flood-tidal delta are implicitly taken into account through its effects on waves and currents (Nienhuis & Ashton, 2016). In that sense, the BRIE-D model, as well as the BRIE model, offers a different picture on inlet and barrier dynamics than that in previous studies, such as that of van de Kreeke (2006).

The overwash transport is assumed to be independent of wave height, which is a simplification of reality. One of the advantages of the BRIE-D model is the low computational effort it requires, involving parametrizations of certain processes. Making overwash dependent on wave height is out of the scope of this study, but we would expect to have more severe drowning for lower wave heights because less sediment would be transported to the top and back of the barrier. We performed a sensitivity analysis on the maximum overwash transport, and saw no important dependencies on the obtained results (not shown).

Another way to assess the model performance would be to perform a global sensitivity and uncertainty analysis relating non-linear interactions of model parameters to model output (e.g., Convertino et al., 2014). Given that we

21699011, 2023, 11, Downloaded from https://agupubs.onlinelibrary.wiley.com/doi/10.1029/2022JF007010 by University Of Twente Finance Department, Wiley Online Library on [06/11/2023]. See the Terms and Conditions (https://onlinelibrary.wiley.com/terms-and-conditions) on Wiley Online Library for rules of use; OA articles are governed by the applicable Creative Commons License

21699011, 2023, 11, Downloaded from https://agupubs.onlinelibrary.wiley.com/doi/10.1029/2022JF007010 by University Of Twente Finance Department, Wiley Online Library on [06/11/2023]. See the Terms and Conditions (https://onlinelibrary.wiley.com/terms-and-conditions) on Wiley Online Library for rules of use; OA articles are governed by the applicable Creative Commons License

focused on understanding barrier drowning, rather than the interactions between model parameters and output, this is out of the scope of the present study.

We have studied barrier drowning through the alongshore extent of the barrier below MSL due to tide-wave imbalance, ΔF. We chose this definition because it is straightforward to calculate and easy to compare to observations. Yet, barrier response to high rates of RSLR also includes a decrease in barrier height and width. The latter effect was considered by computing barrier width over time. The decrease in barrier height has not been quantified in this study, but given that it eventually yields drowning of portions of the barrier, it is mainly implicitly included when computing ΔF. Other ways of quantifying barrier drowning could have been based on the computation of aerial barrier area or volume. These are out of the scope of this study.

The BRIE-D model is a useful tool to understand the different mechanisms involved in barrier island evolution and, particularly, drowning. In that sense, it should be seen as an "exploratory model" (Murray, 2003), aiming to understand a poorly understood phenomenon (drowning), rather than simulate any barrier system specifically. Specifically, the multiple parametrizations used in the model make it very computationally efficient, allowing for an in-depth study of the effects of multiple parameters on the response of barrier systems. More observations are needed to properly evaluate and compare projections from BRIE-D, also in comparison with more process-based models, such as that of Mariotti and Hein (2022).

5. Conclusions

Here we aimed to (a) understand the effects of RSLR on the barrier island sediment balance, inlet expansion, and the related barrier drowning, (b) examine the temporal evolution of a barrier island while drowning, as well as quantifying drowning timescales, and (c) explore its dependence on model parameters. With our new model (BRIE-D), we performed simulations with a wide range of values for significant wave height H_s and rate of RSLR $\dot{\xi}$. From model outputs, we studied barrier island drowning by computing the fraction of barrier alongshore extent below MSL, that caused by tide-wave imbalance, the alongshore mean of the barrier width, and the number of inlets.

We found large effects of inlet dynamics on barrier drowning, making it important to include these effects to study the future of barrier islands. Effects of RSLR on inlets manifest as an increase in inlet width and number. Barriers drown faster in simulations that include feedbacks between tidal inlet dynamics and the cross-shore barrier evolution. Nevertheless, barrier response to changes in rates of RSLR remains slow at timescales of ~100s of years for common barrier characteristics. During this adaptation period, first the barrier loses part of its sediment reservoir through a decrease in barrier width. After this period, barrier width stabilizes but inlets expand until the barrier drowns. Specific timescales for barrier drowning will vary between barrier island chains, and should be interpreted to be general rather than specific.

We expect environments with intermediate wave heights to be most sensitive to RSLR-induced drowning. Lower wave environments have shallower depth of closure and thus respond faster to RSLR. Higher waves trigger two opposed mechanisms: a more frequent inlet closure, and a more severe barrier drowning. The former is caused by the larger amount of sediment imported into the inlet system, whereas the latter is a result of the deeper shoreface toe, which makes a barrier system more prone to drowning.

Appendix A: Default Model Parameters

Unless stated otherwise model parameters take their default values, given in Table A1.

Table A1
Default Values of Model Parameters

Name	Value	Units	Explanation
ρ_w	1,025	kg m^{-3}	Density of water
ω	$1.4 \cdot 10^{-4}$	s^{-1}	Offshore tidal radial frequency
g	9.81	m s^{-2}	Gravitational acceleration
R	1.65	–	Submerged specific gravity of sediment

Table A1
Continued

Name	Value	Units	Explanation
e_s	0.01	–	Suspended sediment transport efficiency factor (LTA14)
c_s	0.01	–	Friction factor (B80)
n	0.05	s m$^{-1/3}$	Manning roughness coefficient
$\dot{\xi}$	10	m yr^{-1}	Rate of RSLR
H_s	1.5	m	Significant wave height in deepwater (M17)
a_0	0.8	m	Offshore tidal amplitude (M17)
T_{storm}	10	yr	Minimum period between inlet forming storms
T_p	10	s	Peak wave period
a	0.8	–	Wave asymmetry (AM06)
h	0.2	–	Wave highness (AM06)
γ_{aspect}	0.005	–	Inlet aspect ratio ($\gamma_{aspect} = D_{inlet}/W_{inlet}$)
u_e	1	m/s	Tidal inlet equilibrium velocity (SZ09)
H_{crit}	2	m	Critical barrier height (LTA14)
$W_{b,crit}$	200	m	Critical barrier width (LTA14)
$Q_{ow,\max}$	50	m^3 m^{-1} yr^{-1}	Maximum overwash transport (LTA14)
$L_{\min}$	5	km	Minimum distance between tidal inlets (R13)
L_b	50	km	Length of barrier chain
$s_{background}$	10^{-3}	–	Background slope (LTA14)
k	0.06	m$^{3/5}$ s$^{-6/5}$	Alongshore sediment transport constant (N15)
Δy	100	m	Alongshore grid spacing
Δt	0.05	yr	Time step

Note. Shortened references are as follows: LTA14 (Lorenzo-Trueba & Ashton, 2014), B80 (Bowen, 1980), M17 (Mulhern et al., 2017), AM06 (Ashton & Murray, 2006), SZ09 (de Swart & Zimmerman, 2009), R13 (Roos et al., 2013), and N15 (Nienhuis et al., 2015).

Appendix B: Sensitivity Analysis

We performed a sensitivity analysis for the main parameters that control the system: tidal amplitude a_0, significant wave height H_s, wave period T_p, rate of relative sea level rise (RSLR) $\dot{\xi}$, wave asymmetry a, inlet aspect ratio γ_{aspect}, storm return period T_{storm}, maximum overwash transport $Q_{ow,\max}$ and the suspended sediment transport efficiency factor e_s, which controls the shoreface transport. We varied each of the parameters around ±50% of their default values and computed the fraction of the barrier alongshore extent below MSL (F) at three different stages: at years 100, 300, and 500 after model spin-up. For each set of parameters we created five realizations, from which we computed F and the standard error of the mean. We found clear patterns and deviations from the default case for only four of the eight parameters: a_0, H_s, $\dot{\xi}$, and γ_{aspect}. We also add the results for T_{storm} given its relevance in inlet formation (see Figure B1). Among these five, largest variations were observed for the significant wave height H_s and the rate of RSLR $\dot{\xi}$. Thus, we decided to study the dependence of the model on these parameters in more detail (see Section 3.3).

21699011, 2023, 11, Downloaded from https://agupubs.onlinelibrary.wiley.com/doi/10.1029/2022JF007010 by University Of Twente Finance Department, Wiley Online Library on [06/11/2023]. See the Terms and Conditions (https://onlinelibrary.wiley.com/terms-and-conditions) on Wiley Online Library for rules of use; OA articles are governed by the applicable Creative Commons License

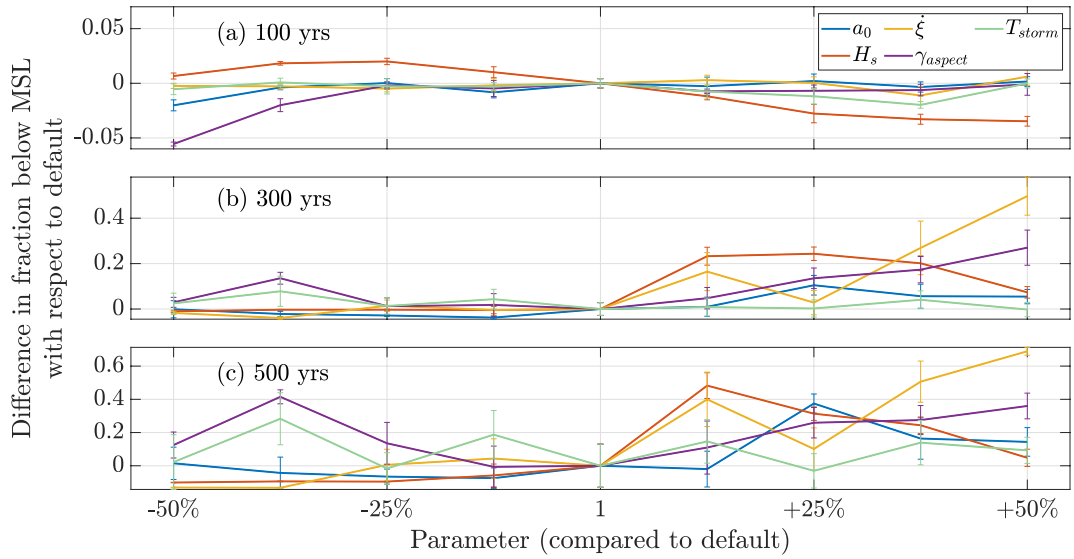

Figure B1. Differences in fraction below mean sea level (MSL) with respect to the default case when varying different morphodynamic parameters at (a) 100, (b) 300, and (c) 500 years after model spin up. Note the different scales in the vertical axis.

Increasing the tidal amplitude, results in a generally larger F due to a gain in tidal prism, which increases the amount of sediment exported by tidal currents (de Swart & Zimmerman, 2009). Lower tidal amplitudes cause a lower F due to less sediment being exported by tidal currents.

Regarding the significant wave height, we observe two opposite responses. Depending on the time after model spin-up, higher waves may produce a decrease or an increase in F. This is explained by distinguishing two processes caused by high waves: (a) higher waves tend to import more sediment into an inlet, thereby favoring its closure (Escoffier, 1940), and (b) higher waves affect the sediment at deeper bed levels, causing a larger depth of closure (Houston, 1995). A larger depth of closure means that a larger volume of sand responds to sea level variations, yielding a system that is more prone to drowning. After 100 years, an increase in significant wave height decreases F to -0.03, while a decrease in H_s increases F up to $+0.02$. This is because at this stage the first mechanism dominates. Nevertheless, after 300 or 500 years of model evolution, when the effects of RSLR-induced drowning are more prevalent, a decrease in H_s causes a decrease in F. There is a clear peak in F for intermediate wave heights. In these situations the second process dominates the evolution of the barrier system, inducing more severe drowning.

Increasing the rate of RSLR results in more severe drowning, inducing an increase in F of up to $+0.68$ by the year 500 for the most extreme case. Note that effects of drowning are only visible from year 300 onwards. In contrast, decreasing the rate of RSLR decreases F by -0.13 because there is less drowning.

An increase in inlet aspect ratio creates narrower inlets for the same cross-sectional area, thereby yielding a slightly lower F at year 100 (-0.01). However, in the years 300 and 500 an increase in inlet aspect ratio results in the opposite effect, yielding an increase in F of up to $+0.36$. Lowering the inlet aspect ratio makes shallower inlets, increasing the bottom friction. This causes the inlets to be more susceptible to closing, decreasing thus F at year 100 by -0.05. However, at 300 or 500 years after model spin-up, F increases for lower values of the inlet aspect ratio. These differences in behavior between earlier and latter times suggest that the dependence of the barrier evolution on the inlet aspect ratio is susceptible to RSLR-driven drowning, similarly to the situation obtained when varying H_s.

The model shows a weak dependency on the storm return period. A decrease in storm return period causes more frequent breaching, yielding a larger F. Larger T_{storm} shows no important differences in F during the first

21699011, 2023, 11, Downloaded from https://agupubs.onlinelibrary.wiley.com/doi/10.1029/2022JF007010 by University Of Twente Finance Department, Wiley Online Library on [06/11/2023]. See the Terms and Conditions (https://onlinelibrary.wiley.com/terms-and-conditions) on Wiley Online Library for rules of use; OA articles are governed by the applicable Creative Commons License

300 years of evolution. At the year 500, a larger T_{storm} seems to suggest a larger F. This asymmetry in behavior means that at this stage the evolution of the barrier system is controlled by RSLR-driven drowning.

Data Availability Statement

The code for the BRIE-D model is accessible from https://doi.org/10.5281/zenodo.7353693 (Portos-Amill et al., 2022).

Acknowledgments
The authors thank Kristen Splinter, Laura J. Moore and two anonymous reviewers for helpful feedback that improved this manuscript.

References

Ashton, A. D., & Lorenzo-Trueba, J. (2018). Morphodynamics of barrier response to sea-level rise. In L. J. Moore & A. B. Murray (Eds.), *Barrier dynamics and response to changing climate* (pp. 277–304). Springer International Publishing. https://doi.org/10.1007/978-3-319-68086-6_9

Ashton, A. D., & Murray, A. B. (2006). High-angle wave instability and emergent shoreline shapes: 1. Modeling of sand waves, flying spits, and capes. *Journal of Geophysical Research*, *111*(F4), F04011. https://doi.org/10.1029/2005JF000422

Beets, D. J., & van der Spek, A. J. F. (2000). The Holocene evolution of the barrier and the back-barrier basins of Belgium and the Netherlands as a function of late Weichselian morphology, relative sea-level rise and sediment supply. *Netherlands Journal of Geosciences – Geologie en Mijnbouw*, *79*(1), 3–16. https://doi.org/10.1017/S0016774600021533

Bowen, A. (1980). Simple models of nearshore sedimentation: Beach profiles and longshore bars. In S. B. McCann (Ed.), *The coastline of Canada* (Vol. 80–10, pp. 1–11). Geological Survey of Canada.

Bricheno, L. M., & Wolf, J. (2018). Future wave conditions of Europe, in response to high-end climate change scenarios. *Journal of Geophysical Research: Oceans*, *123*(12), 8762–8791. https://doi.org/10.1029/2018JC013866

Convertino, M., Muñoz-Carpena, R., Chu-Agor, M. L., Kiker, G. A., & Linkov, I. (2014). Untangling drivers of species distributions: Global sensitivity and uncertainty analyses of MaxEnt. *Environmental Modelling & Software*, *51*, 296–309. https://doi.org/10.1016/j.envsoft.2013.10.001

Davis, R. A., Jr., & FitzGerald, D. M. (2010). Barrier systems. In Blackwell Science Ltd (Ed.), *Beaches and coasts* (pp. 130–166). Wiley.

Deaton, C. D., Hein, C. J., & Kirwan, M. L. (2017). Barrier island migration dominates ecogeomorphic feedbacks and drives salt marsh loss along the Virginia Atlantic Coast, USA. *Geology*, *45*(2), 123–126. https://doi.org/10.1130/G38459.1

de Swart, H., & Zimmerman, J. (2009). Morphodynamics of tidal inlet systems. *Annual Review of Fluid Mechanics*, *41*(1), 203–229. https://doi.org/10.1146/annurev.fluid.010908.165159

Dingler, J. R., Reiss, T. E., & Plant, N. G. (1993). Erosional patterns of the Isles Dernières, Louisiana, in relation to meteorological influences. *Journal of Coastal Research*, 112–125.

Escoffier, F. (1940). The stability of tidal inlets. *Shore and Beach*, *8*(4), 114–115.

FitzGerald, D. M., Fenster, M. S., Argow, B. A., & Buynevich, I. V. (2008). Coastal impacts due to sea-level rise. *Annual Review of Earth and Planetary Sciences*, *36*(1), 601–647. https://doi.org/10.1146/annurev.earth.35.031306.140139

Houston, J. (1995). Beach-fill volume required to produce specified dry beach width. In *Coastal Engineering Technical Note* (pp. 11–32). US Army Engineer Waterways Experiment Station Vicksburg.

Hume, T. M., & Herdendorf, C. E. (1992). Factors controlling tidal inlet characteristics on low drift coasts. *Journal of Coastal Research*, *8*(2), 355–375.

Leatherman, S. P. (1983). Barrier dynamics and landward migration with Holocene sea-level rise. *Nature*, *301*(5899), 415–417. https://doi.org/10.1038/301415a0

Lorenzo-Trueba, J., & Ashton, A. D. (2014). Rollover, drowning, and discontinuous retreat: Distinct modes of barrier response to sea-level rise arising from a simple morphodynamic model. *Journal of Geophysical Research: Earth Surface*, *119*(4), 779–801. https://doi.org/10.1002/2013JF002941

Lorenzo-Trueba, J., & Mariotti, G. (2017). Chasing boundaries and cascade effects in a coupled barrier-marsh-lagoon system. *Geomorphology*, *290*, 153–163. https://doi.org/10.1016/j.geomorph.2017.04.019

Mariotti, G., & Hein, C. J. (2022). Lag in response of coastal barrier-island retreat to sea-level rise. *Nature Geoscience*, *15*(8), 633–638. https://doi.org/10.1038/s41561-022-00980-9

Mellett, C. L., & Plater, A. J. (2018). Drowned barriers as archives of coastal-response to sea-level rise. In L. J. Moore & A. B. Murray (Eds.), *Barrier dynamics and response to changing climate* (pp. 57–89). Springer International Publishing. https://doi.org/10.1007/978-3-319-68086-6_2

Moore, L. J., List, J. H., Williams, S. J., & Stolper, D. (2010). Complexities in barrier island response to sea level rise: Insights from numerical model experiments, North Carolina Outer Banks. *Journal of Geophysical Research*, *115*(F3), F03004. https://doi.org/10.1029/2009JF001299

Mulhern, J. S., Johnson, C. L., & Martin, J. M. (2017). Is barrier island morphology a function of tidal and wave regime? *Marine Geology*, *387*, 74–84. https://doi.org/10.1016/j.margeo.2017.02.016

Murray, A. B. (2003). Contrasting the goals, strategies, and predictions associated with simplified numerical models and detailed simulations. *Geophysical Monograph-American Geophysical Union*, *135*, 151–168.

Nienhuis, J. H., & Ashton, A. D. (2016). Mechanics and rates of tidal inlet migration: Modeling and application to natural examples. *Journal of Geophysical Research: Earth Surface*, *121*(11), 2118–2139. https://doi.org/10.1002/2016JF004035

Nienhuis, J. H., Ashton, A. D., & Giosan, L. (2015). What makes a delta wave-dominated? *Geology*, *43*(6), 511–514. https://doi.org/10.1130/G36518.1

Nienhuis, J. H., & Lorenzo-Trueba, J. (2019). Simulating barrier island response to sea level rise with the barrier island and inlet environment (BRIE) model v1.0. *Geoscientific Model Development*, *12*(9), 4013–4030. https://doi.org/10.5194/gmd-12-4013-2019

Ortiz, A. C., & Ashton, A. D. (2016). Exploring shoreface dynamics and a mechanistic explanation for a morphodynamic depth of closure. *Journal of Geophysical Research: Earth Surface*, *121*(2), 442–464. https://doi.org/10.1002/2015JF003699

Palmer, M. D., Gregory, J. M., Bagge, M., Calvert, D., Hagedoorn, J. M., Howard, T., et al. (2020). Exploring the drivers of global and local sea-level change over the 21st century and beyond. *Earth's Future*, *8*(9), e2019EF001413. https://doi.org/10.1029/2019EF001413

Pickering, M., Wells, N., Horsburgh, K., & Green, J. (2012). The impact of future sea-level rise on the European Shelf tides. *Continental Shelf Research*, *35*, 1–15. https://doi.org/10.1016/j.csr.2011.11.011

Portos-Amill, L., Nienhuis, J. H., & de Swart, H. (2022). LPortos-Amill/BRIE-D: BRIE-D model (v1.0) [Software]. Zenodo. https://doi.org/10.5281/zenodo.7353693

21699011, 2023, 11, Downloaded from https://agupubs.onlinelibrary.wiley.com/doi/10.1029/2022JF007010 by University Of Twente Finance Department, Wiley Online Library on [06/11/2023]. See the Terms and Conditions (https://onlinelibrary.wiley.com/terms-and-conditions) on Wiley Online Library for rules of use; OA articles are governed by the applicable Creative Commons License

Reef, K. R. G., Roos, P. C., Andringa, T. E., Dastgheib, A., & Hulscher, S. J. M. H. (2020). The impact of storm-induced breaches on barrier coast systems subject to climate change—A stochastic modelling study. *Journal of Marine Science and Engineering*, *8*(4), 271. https://doi.org/10.3390/jmse8040271

Roos, P. C., Schuttelaars, H. M., & Brouwer, R. L. (2013). Observations of barrier island length explained using an exploratory morphodynamic model. *Geophysical Research Letters*, *40*(16), 4338–4343. https://doi.org/10.1002/grl.50843

Sanders, J. E., & Kumar, N. (1975). Evidence of shoreface retreat and in-place "drowning" during Holocene submergence of barriers, shelf off Fire Island, New York. *Geological Society of America Bulletin*, *86*(1), 65–76. https://doi.org/10.1130/0016-7606(1975)86<65:eosrai>2.0.co;2

Stolper, D., List, J. H., & Thieler, E. R. (2005). Simulating the evolution of coastal morphology and stratigraphy with a new morphological-behaviour model (GEOMBEST). *Marine Geology*, *218*(1), 17–36. https://doi.org/10.1016/j.margeo.2005.02.019

van de Kreeke, J. (2004). Equilibrium and cross-sectional stability of tidal inlets: Application to the Frisian inlet before and after basin reduction. *Coastal Engineering*, *51*(5), 337–350. https://doi.org/10.1016/j.coastaleng.2004.05.002

van de Kreeke, J. (2006). An aggregate model for the adaptation of the morphology and sand bypassing after basin reduction of the Frisian Inlet. *Coastal Engineering*, *53*(2), 255–263. https://doi.org/10.1016/j.coastaleng.2005.10.013

References From the Supporting Information

Ashton, A. D., Murray, A. B., & Arnoult, O. (2001). Formation of coastline features by large-scale instabilities induced by high-angle waves. *Nature*, *414*, 296–300. https://doi.org/10.1038/35104541

Brown, E. I. (1928). Inlets on sandy coasts. *Proceedings of the American Society of Civil Engineers*, *54*, 505–554.

Ferguson, R., & Church, M. (2004). A simple universal equation for grain settling velocity. *Journal of Sedimentary Research*, *74*(6), 933–937. https://doi.org/10.1306/05120474093

Longuet-Higgins, M. S., & Stewart, R. (1962). Radiation stress and mass transport in gravity waves, with application to 'surf beats'. *Journal of Fluid Mechanics*, *13*(4), 481–504. https://doi.org/10.1017/S0022112062000877

Powell, M. A., Thieke, R. J., & Mehta, A. J. (2006). Morphodynamic relationships for ebb and flood delta volumes at Florida's tidal entrances. *Ocean Dynamics*, *56*(3), 295–307. https://doi.org/10.1007/s10236-006-0064-3

Terra, G. M., van de Berg, W. J., & Maas, L. R. (2005). Experimental verification of Lorentz' linearization procedure for quadratic friction. *Fluid Dynamics Research*, *36*(3), 175–188. https://doi.org/10.1016/j.fluiddyn.2005.01.005

21699011, 2023, 11, Downloaded from https://agupubs.onlinelibrary.wiley.com/doi/10.1029/2022JF007010 by University Of Twente Finance Department, Wiley Online Library on [06/11/2023]. See the Terms and Conditions (https://onlinelibrary.wiley.com/terms-and-conditions) on Wiley Online Library for rules of use; OA articles are governed by the applicable Creative Commons License